SAND2021-7638C

The Effects of Inverter Clipping and Curtailment-Inducing Grid Support Functions on PV Planning Decisions

Joseph A. Azzolini and Matthew J. Reno

Sandia National Laboratories, Albuquerque, NM, 87185, USA

***Abstract*—Recent trends in PV economics and advanced inverter functionalities have contributed to the rapid growth in PV adoption; PV modules have gotten much cheaper and advanced inverters can deliver a range of services in support of grid operations. However, these phenomena also provide conditions for PV curtailment, where high penetrations of distributed PV often necessitate the use of advanced inverter functions with VAR priority to address abnormal grid conditions like over- and under-voltages. This paper presents a detailed energy loss analysis, using a combination of open-source PV modeling tools and high-resolution time-series simulations, to place the magnitude of clipped and curtailed PV energy in context with other operational sources of PV energy loss. The simulations were conducted on a realistic distribution circuit, modified to include utility load data and 341 modeled PV systems at 25% of the customer locations. The results revealed that the magnitude of clipping losses often overshadows that of curtailment but, on average, both were among the lowest contributors to total annual PV energy loss. However, combined clipping and curtailment loss are likely to become more prevalent as recent trends continue.**

***Keywords*—advanced inverter functions, autonomous Volt-VAR, clipping, curtailment, energy yield analysis, quasi-static time-series (QSTS)**

I. Introduction

Recent trends in photovoltaic (PV) economics and advanced inverter functionalities have contributed to the rising penetration levels of PV systems in distribution circuits throughout the country. Understanding the effects of these trends is a critical step to ensure the continued transition towards a more sustainable energy landscape. Over time, the cost breakdowns of PV systems change in response to technological advances and policy decisions. As some aspects of PV systems become more expensive relative to others, research and planning tasks must be reevaluated to ensure resources are being utilized for the greatest impact.

Over the past several years, the reduction in PV module prices relative to other hardware components has led to changes in PV system design. Specifically, the relatively low cost of PV modules compared to PV inverters has resulted in PV arrays being increasingly oversized [1], and rated efficiencies of commercially available PV modules and inverters have each continued to improve [2]. The result of these trends is that the DC/AC ratios of installed PV systems have been steadily increasing. While a higher DC/AC ratio does provide benefits (e.g., reduced upfront costs and reduced AC output variability), more energy is "lost" to the effects of clipping as the inverter spends more time operating at full capacity. Although clipping is more accurately described as an under-utilization of available energy, for the sake of simplicity it will be referred to as a source of energy loss in this work.

The implementation of advanced inverter functions to help regulate conditions on the grid is another growing trend that has the potential to impact PV energy yields. All new PV inverters that connect to the grid are required to have built-in capabilities for a variety of grid support functions, as defined in the IEEE 1547 standard [3]. These functions are proving to be invaluable tools for enabling high PV penetrations [4]. The downside is that, under certain conditions, PV real power must be sacrificed – or curtailed – to fulfill the requirements of the grid support functions with VAR priority [3]. Therefore, when PV inverters are operating at or near full capacity (as is increasingly the case due to high DC/AC ratios), they are more likely to curtail real power to provide reactive power support. Similar to clipping, curtailment of real PV power is not technically a "loss" in the traditional sense but will be referred to as a loss in the context of this paper.

In addition to clipping and curtailment, there are a variety of other operational loss mechanisms present in PV systems. These losses are often categorized as optical losses (e.g., reflection, soiling, and shading), DC system losses (e.g., module mismatch, temperature effects, and connections), and AC systems losses (e.g., inverter efficiency, clipping, and wiring). Many of these loss types vary with atmospheric conditions, but many are also interdependent. For example, as particles accumulate on the surface of the modules in a PV array (i.e., increasing levels of soiling), the DC power output is reduced, which changes the operating point and instantaneous efficiency of the inverter. In that same example, the soiling would also reduce the current on the DC side of the system, potentially reducing the module temperatures and increasing DC power. Fortunately, decades of research has been performed to generate accurate models for various aspects of solar PV systems, and there are a variety of open-source tools and databases available that can be utilized to analyze the different sources of PV energy loss.

Unlike other sources of energy loss that can be estimated by analyzing meteorological data and PV array designs, curtailment losses are dependent on both atmospheric conditions and grid conditions to which the PV system is connected. Therefore, calculating curtailment requires detailed models of the electrical distribution system, including knowledge of network topologies, voltage regulation

equipment, load characteristics, and energy consumption profiles. Since the grid parameters that influence curtailment (e.g., voltage at the PV system's point of interconnection) change throughout time, quasi-static time-series (QSTS) simulations of distribution circuits are often required [5]. QSTS simulations are able to capture the time-varying and time-dependent circuit metrics by solving a series of sequential power flows, where the converged states of one iteration serve as the initial states of the power flow at the next time step.

The goal of this study is to investigate the impacts of growing trends, like high DC/AC ratios and grid support functions, on PV energy yields through detailed PV modeling and QSTS simulations of a realistic distribution system with hundreds of interconnected PV systems. This methodology enables grid-dependent sources of energy loss (i.e., curtailment) to be accounted for directly compared to conventional sources of operational PV energy losses. Understanding the relative magnitudes of these losses will help to inform future decisions for PV system owners, solar developers, and grid planners.

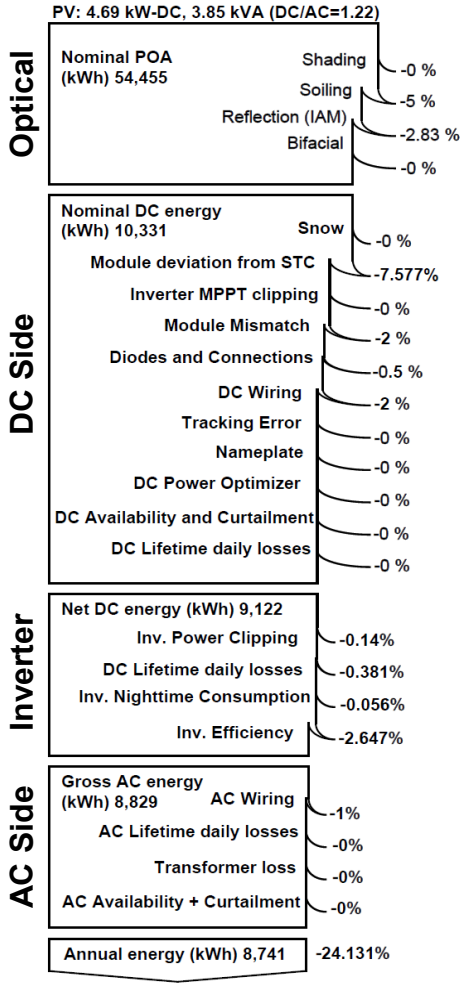

Fig. 1. Loss diagram for default residential PV system in SAM [6].

II. Background

There are many sources of energy loss in PV systems that occur throughout the absorption, conversion, and transmission processes, each ultimately affecting the number of photons that end up as available electrons to perform electrical work in a circuit. Since energy losses have a direct effect on the economics of a PV system, it is important to understand the common sources of energy loss, as well as their relative magnitudes to one another. Software packages for PV system design often include loss diagrams that identify each source of loss being accounted for and which part of the system it is applied to. In Fig. 1, an example loss diagram was generated using the System Advisor Model (SAM) software [6] for a residential PV system with all parameters set to their default values. The PV system in this example had a 4.69 kW PV array and a 3.85 kVA inverter, meaning it had a DC/AC ratio of 1.22.

As shown in Fig. 1, all the different sources of loss are converted to energy values (in kWh) so that they can be compared using the same units. The losses are organized by the order in which they take effect, starting with optical losses at the plane-of-array (POA) and ending with AC losses. For the PV system in Fig. 1, the largest source of loss was module deviation from standard test conditions (STC), which accounts for the effects of module temperature. The next largest losses in order are soiling, reflection, and inverter efficiency loss, and the total energy loss was 24.131%. These results can be used as a resource when evaluating the economic decisions associated with PV system design, and they highlight the PV system components to target with future research projects.

III. Methods

The energy analysis in this study was carried out using a combination of QSTS simulations and open-source PV modeling tools to evaluate the operational power losses for a collection of hundreds of PV systems. Being that many of the sources of PV energy losses are inter-dependent, and each loss type can be influenced by a variety of modeling parameters and assumptions, the intent of this work was to capture the relative magnitudes of each loss type rather than to perform an exhaustive sensitivity analysis. Therefore, detailed PV models were utilized whenever possible, but some simplifications and constant loss factors were applied to streamline the analysis of the hundreds of PV systems. The following subsections provide additional details about the test circuit used in the QSTS distribution system simulations, and a detailed accounting of the PV modeling steps and types of losses that were evaluated.

A. Distribution System Modeling

Yearlong QSTS simulations were performed on a realistic distribution circuit to quantify the magnitude of PV energy lost to curtailment when an inverter's grid support function was enabled. In this study, the autonomous Volt-VAR function was selected as the curtailment-inducing, grid support function to be analyzed in this paper. When this function is enabled, a PV system will autonomously inject or absorb reactive power based on the voltage at its point of interconnection to help prevent extreme voltage conditions. This function operates with VAR priority, meaning if an inverter is operating at its kVA limit, it will curtail real power to provide additional reactive power, if necessary. Several studies and pilot programs have validated the benefits of implementing the autonomous Volt-VAR function to help regulate voltages throughout distribution circuits [7, 8]. For this study, the IEEE 1547 Category B default Volt-VAR settings [3] were used and programmed into the built-in PV inverter model in OpenDSS.

All QSTS simulations were conducted on a modified version of the EPRI Ckt5 test circuit [9], shown in Fig. 2, using OpenDSS via the GridPV toolbox [10]. This circuit represents an actual 12.47 kV distribution circuit with a maximum bus distance from the substation of 3.24 miles. Each of the 1,379 loads was assigned a unique time-series profile of real and reactive power values based on 1-minute, anonymized utility data from customers in Austin, Texas. This test circuit was selected in part because of this high-resolution load data; previous work has shown that loading conditions can significantly influence PV curtailment [11, 12]. Since the original test circuit did not contain any PV systems, 25% of customer locations (341 in total) were selected at random to have a PV system added (identified as yellow stars in Fig. 2). This random distribution ensured that the PV systems would be located at a variety of distances from the substation, thus capturing the effects of voltage drops along the feeder on PV curtailment.

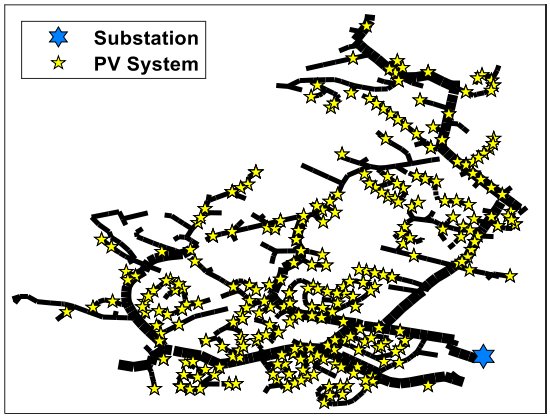

Fig. 2. Circuit plot of modified EPRI Ckt5 with 341 PV systems.

In the QSTS simulations, each PV system was assigned a time-series unique generation profile that dictated its real power output at each point in time. These time-series profiles represented the AC power output from the PV inverters after all other losses had been subtracted out (see subsection B for more details on the PV time-series modeling). Therefore, the PV outputs from the QSTS results with autonomous Volt-VAR enabled could be subtracted from the original AC output profiles to calculate curtailment losses.

Note that the results in this paper are dependent on the distribution system, penetration level, and autonomous Volt-VAR settings used. While the rest of the energy losses are independent of the distribution system QSTS simulation, the curtailment is directly related to the local voltage at each PV system. In feeders with high voltages, higher penetrations of PV, or PV with more aggresive Volt-VAR settings, the curtailment losses could be higher.

B. PV Modeling

After the PV locations throughout the distribution circuit were selected, the orientation and ratings were determined for each PV system. First, the PV array orientations (i.e., tilt and azimuth angles) were selected for each PV system out of 21 different options according to the distributions provided by the rooftop PV suitability database [13] for Austin, Texas, which contains the total suitable roof area at a variety of tilt and azimuth angles for every zip code in the US. Next, the inverter kVA ratings were determined for each system based on the annual energy demand of the customer at that location. In other words, the kVA ratings were selected with the goal of net-zero energy consumption at all PV locations, resulting in the distribution ratings and energy yields (from the QSTS simulation) presented in Fig. 3. Lastly, based on recent trends in PV installation data [1], a DC/AC ratio of 1.2 was applied to all PV systems to set their DC ratings.

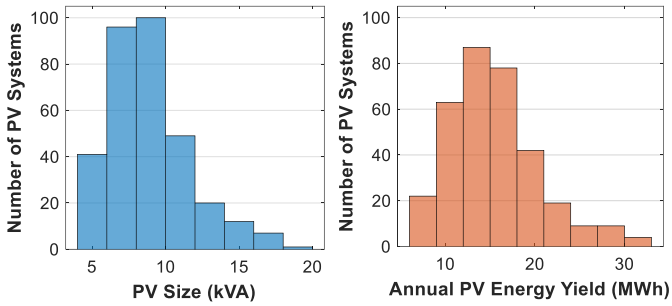

Fig. 3. Histogram of kVA ratings (left) and annual energy yields of all PV systems (right) on the distribution feeder.

After the PV systems had been sized and assigned an array orientation, their time-series power outputs and losses were calculated using a combination of open-source modeling tools and databases, including the National Solar Resource Database (NSRDB) [14], the PVLIB toolbox [15], equations from the PV Performance Modeling Collaborative (PVPMC) [16], the System Advisor Model (SAM) software [6], and PVWatts [17]. The constant loss factors used in several of the modeling steps were also derived from default values used by these open-source tools. A detailed procedure for modeling the output power and losses for each PV system is presented in Table 1, which includes references to specific models and equations. Unless otherwise stated, default parameters and settings were used for all models and functions. Characteristics from a representative PV module (Trina Solar TSM-365DD14A) and inverter (SMA SB7.7-1TP-US-41) were also utilized in Table 1. The procedure in Table 1 was applied to generate unique AC power output profiles for all PV systems, which were then imported into the OpenDSS circuit model.

For the energy loss analysis, all types of losses were converted to their equivalent kW value so that all losses could be compared using the same units. Table 2 identifies all the loss types that were analyzed and the corresponding modeling steps from Table 1 where each loss type was calculated. It should be noted that referring to some of the effects in Table 2 as a "loss" may be a misnomer, as they may increase power under certain circumstances. Nevertheless, for the sake of this analysis, the terms "loss" and "negative loss" will be employed.

The loss types in Table 2 account for optical losses, DC system losses, and AC system losses. The optical losses capture the effects of reflection (photons that reach the PV module but are not absorbed), spectral mismatch (difference in the outdoor spectrum of the light source compared to testing conditions), shading (obstruction of photons from reaching the PV module), and soiling (the accumulation of particles on a PV module that limits incoming photons). The DC system losses capture the

impacts of PV module temperature (where values higher than the test conditions reduce power output, and vice versa), PV module mismatch (where current is limited by the lowest current module in a string and voltage is limited by the lowest voltage string in an array), and conduction (where voltage drops occur across bypass diodes, connectors, and conductors). The AC system losses capture the inverter losses due to its cut in/out threshold (power level at which the inverter shuts off), efficiency curve (changes in inverter performance based on power level), clipping threshold (max kVA limit), and autonomous Volt-VAR function (VAR-priority, grid support function that curtails real power). It was assumed that power was being measured at the inverter terminals, meaning AC wiring loss could be neglected.

TABLE 1. PV MODELING PROCEDURE

#	Description
1.	Download 30-min, 2019 irradiance and weather data for Austin, TX [14]
2.	Calc. sun position using *pvl_spa* [15]
3.	Calc. extraterrestrial radiation using *pvl_extraradiation* [15]
4.	Calc. angle of incidence (*AOI*) using *pvl_getaoi* [15]
5.	Calc. air mass using *pvl_relativeairmass* and *Pvl_absoluteairmass* [15]
6.	Calc. beam component (E_b) using DNI x cos(*AOI*) [16]
7.	Calc. sky diffuse (E_d) using *pvl_perez* [15]
8.	Calc. ground diffuse (E_g) using *pvl_grounddiffuse* [15]
9.	Calc. total POA irradiance (E_{POA}) using $E_{POA}=E_b+E_d+E_g$ [16]
10.	Apply incident angle modifier for reflection using *pvl_phsyicaliam* [15]
11.	Adjust for spectral mismatch using *pvl_FSspeccorr* [15]
12.	Apply shading loss factor of 3% [17]
13.	Apply soiling loss factor of 1% [18]
14.	Convert irradiance to per unit with a base of 1000 W/m^2 then multiply by DC rating of the PV array to convert to kW
15.	Calc. module temperature using *pvl_sapmcell* [15]
16.	Adjust for module temperature by applying -0.3718 %/°C (based on Trina Solar TSM-365DD14A module)
17.	Apply DC mismatch loss factor of 2% [17]
18.	Apply loss factor of 2.5% for DC wiring, connections, and diodes [17]
19.	Apply inverter cut in/out threshold of 0.3% (based on SMA SB7.7-1TP-US-41 inverter)
20.	Apply inverter efficiency curve using *pvl_snlinverter* [15] (based on SMA SB7.7-1TP-US-41 inverter)
21.	Adjust for inverter clipping by setting max. AC output = kVA rating
22.	Linearly interpolate to 1-min resolution for the QSTS simulations

TABLE 2. PV LOSS TYPE AND CALCULATION

Loss Type	Calculation (Step # Refers to *Table 1*)
Reflection*	Subtract Step 10 results from Step 9
Spectral Mismatch*	Subtract Step 11 results from Step 10
Shading*	Subtract Step 12 results from Step 11
Soiling*	Subtract Step 13 results from Step 12
Mod. Temperature	Subtract Step 16 results from Step 13
Mod. Mismatch	Subtract Step 17 results from Step 16
DC Conduction	Subtract Step 18 results from Step 17
Inv. Cut In/Out	Subtract Step 19 results from Step 18
Inv. Efficiency	Subtract Step 20 results from Step 19
Inv. Clipping	Subtract Step 21 results from Step 20
Curtailment	Run QSTS simulation and record PV power outputs. Subtract those results from Step 21

**all optical losses converted to kW using Step 14*

Other types of losses can be modeled as well. For instance, we assumed that the PV systems were all new installations, but PV system performance does degrade over time. Other potential sources of loss, like the maximum power point tracking (MPPT) performance, have been shown to have a minimal effect on PV output [19] and were neglected. So while it is not an entirely exhaustive accounting, the loss types captured in this analysis were sufficient to satisfy the objective of this work.

IV. RESULTS

To help visualize the impacts that each loss type from Table 2 had on PV power output, time-series values were stored after each of the corresponding modeling steps from Table 1 for one of the PV systems and converted to kilowatt values. Two consecutive days were selected at random and plotted as a time-series in Fig. 4. The legend entries in this figure refer to the resulting power outputs after each corresponding loss was accounted for, in the same order as Table 1. For example, in the middle of the first day (January 19th) after clipping loss was accounted for, the power output was reduced to 10.57 kW due to the capacity limit of the inverter. For much of the time that the inverter spent operating at its maximum capacity on this day, curtailment losses were also observed. This behavior was in line with expectations and observations from previous work [11], as the conditions during this time were likely to induce curtailment—the inverter was already operating at maximum capacity, and the load during the wintertime was much lower than its summer peak, so the inverter attempted to reduce the over-voltage by curtailing active power to absorb reactive power. Similar conditions were observed in Fig. 4 on the following day but were more difficult to distinguish due to the irradiance variability on that day.

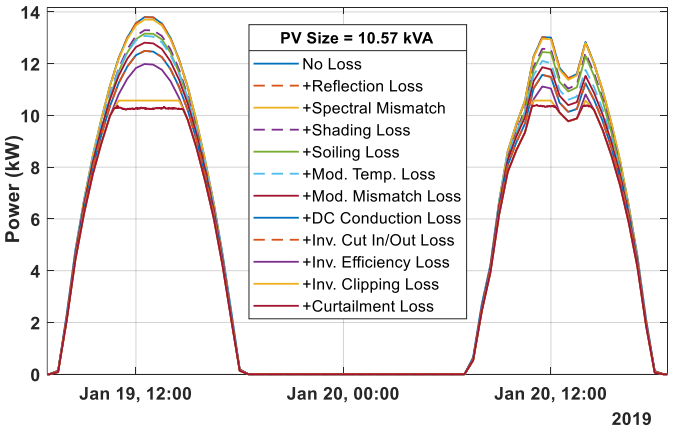

Fig. 4. Example of PV power losses over two consecutive days. This PV system had a tilt angle of 41° and an azimuth angle of 180°.

To further clarify these relationships, and to place the losses in more intuitive terms, the results in Fig. 4 were magnified in the top subplot of Fig. 5 and converted to percentages of the *No Loss* time-series in the bottom subplot of Fig. 5. In other words, the *Inv. Clipping Loss* line in the bottom subplot represents the difference between the *+Inv. Efficiency Loss* line and the *+Inv. Clipping Loss* line as a percentage of the *No Loss* line. Overall, the bottom subplot of Fig. 5 highlights the time-varying behavior of each loss type. For instance, on this day between roughly 10:30 AM and 3:00 PM, clipping loss and curtailment

loss reached maximum values of 10.23% and 2.72%, respectively, but did not contribute any power loss throughout the rest of the day. Other types of losses, like module mismatch or DC conduction losses, do not appear to change much over time because they were modeled as constant loss factors (see Table 1). This subplot also shows examples of "negative loss" associated with PV module temperature and spectral mismatch. For the temperature effects, this behavior indicates that for those time points the module temperature was colder than 25°C (which is the standard test condition value reports for PV modules), causing an increase in power output relative to its nominal rating. For the spectral mismatch effects, typical values of the spectral mismatch multiplier are in the range of 0.95 to 1.05 (based on PV cell type, absolute air mass, and the precipitable water content of the air). Therefore, the spectral mismatch multiplier for those time points was above 1, leading to a relative increase in output power, or negative loss.

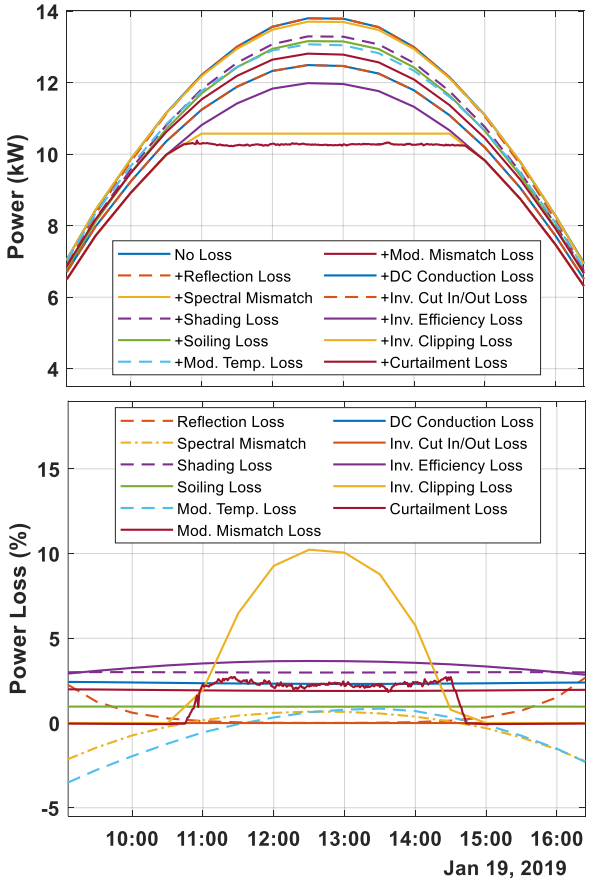

Fig. 5. Magnified power time-series from Fig. 4 (top) and corresponding power loss percentages (bottom) on January 19th.

The calculations outlined in Table 2 defined all the losses as kilowatt values over time. Those values were converted to energy values (MWh) and summed for each of the 341 PV systems. In Fig. 6, the annual energy loss totals of all PV systems were categorized by type and presented as box plot distributions, where the red line represents the median value and the bottom and top edges of the box represent the 25th and 75th percentiles, respectively. Since the results in Fig. 6 are presented in terms of total energy loss, the variability within each loss type is mostly driven by the distribution of PV sizes, but also contains some degree of variability that is attributed to the inter-dependent nature of the losses, as discussed in the introduction of the paper. Despite accounting for some of the highest values of instantaneous losses in Fig. 5, the results in Fig. 6 indicate that annual clipping and curtailment losses were among the lowest of all loss types being analyzed. Fig. 6 also reveals that spectral mismatch caused some of the PV systems to experience a net negative loss. Similar to the discussion of Fig. 5, typical values of the spectral mismatch multiplier are in the range of 0.95 to 1.05 and are applied to the POA irradiance, so it reasonable that some PV systems experienced a net positive effect from spectral mismatch on their energy yields.

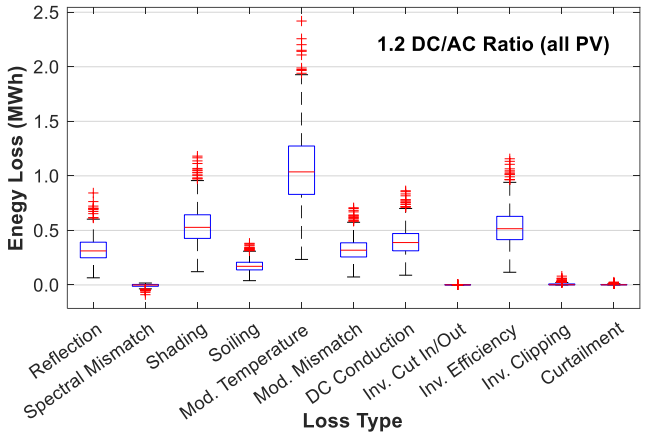

Fig. 6. Box plot of energy losses (MWh) for each of the 341 PV systems categorized by loss type from Table 2.

As noted in Fig. 6, all PV systems had a common DC/AC ratio of 1.2. Since the recent trends in PV economics have favored increasing DC/AC ratios over the past few years, additional analyses were performed to investigate the impact of modifying the DC/AC to 1.3 for all PV systems. The modeling procedure in Table 1 was repeated after multiplying the kVA ratings by 1.3 (i.e., holding the AC side constant), and another QSTS simulation was conducted. The power losses were calculated according to Table 2, converted to annual energy loss totals. The average annual energy loss was then calculated for each type (for both sets of results) and converted to a percentage of total POA energy. These results, presented as a bar chart in Fig. 7, show that while clipping, curtailment, and inverter efficiency losses all increased with the DC/AC ratio, the changes were marginal, with the total average losses increasing from 18.25% to 18.57%.

The results in Fig. 7 revealed that increasing the DC/AC ratio of the PV systems does not impact any of the average optical or DC system losses. Therefore, a more apt approach of interpreting the results may be to compare the clipping and curtailment losses as a percentage of energy available at input terminals of the inverters rather than to the total POA energy before losses, thus magnifying their effects. This perspective may be useful to customers when evaluating a new PV installation. For example, if a customer is constrained by a limited area on their roof, it may be prudent for them to factor in any potential increases in clipping and curtailment losses associated with different sized inverters.

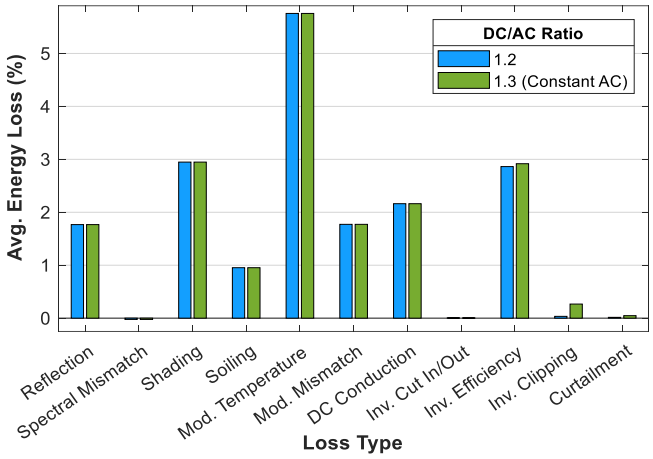

Fig. 7. Bar chart of energy losses (%) by loss type and DC/AC ratio for each of the 341 PV systems.

V. Conclusion

Recent trends in PV economics have led to changes in the ways that PV systems are designed and operated. Specifically, PV module prices have been disproportionately reduced compared to PV inverter prices, while the rated efficiencies of both have continued to improve. These factors have both contributed to the rising DC/AC ratios of installed PV systems in recent years, which often leads to increased clipping losses and provides more opportunity for curtailment to occur when grid support functions are enabled. Understanding the relative magnitudes of each major source of energy loss in PV systems not only helps to inform future research pathways but informs decision-making for a variety of solar energy stakeholders.

To address this challenge, a detailed energy loss analysis was performed using a variety of open-source PV modeling tools and QSTS simulations conducted on a realistic distribution network with real utility loading data for all customer locations. A total of 341 PV systems were placed randomly throughout the distribution circuit and set to operate in autonomous Volt-VAR mode with VAR priority to induce curtailment. Detailed time-series models were generated for each PV system with various loss mechanisms identified and evaluated. After repeated the analyses for the two different DC/AC ratios, it was observed that:

- Clipping and curtailment losses had high instantaneous values but were among the smallest sources of total annual energy loss
- Total average losses were 18.25% and 18.57% for DC/AC ratios of 1.2 and 1.3, respectively
- During PV system design, if the DC size rating has already been determined, accounting for clipping and curtailment losses (including performing distribution system QSTS simulations) may help in determining the AC rating of the system

Overall, while the magnitude of clipping and curtailment losses are still relatively low, they are likely to increase as recent trends continue and more grid support functions are required from PV inverters.

Acknowledgment

Sandia National Laboratories is a multi-mission laboratory managed and operated by National Technology and Engineering Solutions of Sandia, LLC., a wholly owned subsidiary of Honeywell International, Inc., for the U.S. Department of Energy's National Nuclear Security Administration under contract DE-NA-0003525.

References

[1] G. Barbose, N. R. Darghouth, S. Elmallah, S. Forrester *et al.*, "Tracking the Sun: Pricing and Design Trends for Distributed Photovoltaic Systems in the United States," Lawrence Berkeley National Laboratory, 2019.

[2] F. Baumgartner, "5 - Photovoltaic (PV) balance of system components: Basics, performance," in *The Performance of Photovoltaic (PV) Systems*, N. Pearsall Ed.: Woodhead Publishing, 2017, pp. 135-181.

[3] *IEEE 1547 Standard for Interconnection and Interoperability of Distributed Energy Resources with Associated Electric Power Systems Interfaces*, IEEE, 2018.

[4] J. Seuss, M. J. Reno, R. J. Broderick, and S. Grijalva, "Analysis of PV Advanced Inverter Functions and Setpoints under Time Series Simulation," Sandia National Laboratories, SAND2016-4856, 2016.

[5] J. Deboever, S. Grijalva, M. J. Reno, and R. J. Broderick, "Fast Quasi-Static Time-Series (QSTS) for yearlong PV impact studies using vector quantization," *Sol Energy,* vol. 159, pp. 538-547, 2018.

[6] *System Advisor Model Version 2020.11.29 (SAM 2020.11.29)*. National Renewable Energy Laboratory, Golden, CO. [Online]. Available: https://sam.nrel.gov

[7] J. Giraldez, A. Hoke, P. Gotseff, N. Wunder *et al.*, "Advanced Inverter Voltage Controls: Simulation and Field Pilot Findings," National Renewable Energy Laboratory, 2018.

[8] H. V. Haghi, Z. Pecenak, J. Kleissl, J. Peppanen *et al.*, "Feeder Impact Assessment of Smart Inverter Settings to Support High PV Penetration in California," in *2019 IEEE Power & Energy Society General Meeting (PESGM)*, 4-8 Aug. 2019 2019, pp. 1-5, doi: 10.1109/PESGM40551.2019.8974016.

[9] EPRI, "Enhanced Load Modeling: Leveraging Expanded Monitoring and Metering," Palo Alto, CA, 3002015283, 2019.

[10] M. J. Reno and K. Coogan, "Grid Integrated Distributed PV (GridPV) Version 2," Sandia National Labs, SAND2014-20141, 2014.

[11] J. A. Azzolini, M. J. Reno, and K. A. W. Horowitz, "Evaluation of Curtailment Associated with PV System Design Considerations," in *IEEE PES General Meeting*, 2020.

[12] J. A. Azzolini and M. J. Reno, "Impact of Load Allocation and High Penetration PV Modeling on QSTS-Based Curtailment Studies," in *IEEE PES General Meeting*, 2021.

[13] P. Gagnon, R. Margolis, and C. Phillips. *Rooftop Photovoltaic Technical Potential in the United States*, doi: 10.7799/1575064.

[14] M. Sengupta, Y. Xie, A. Lopez, A. Habte, G. Maclaurin, and J. Shelby, "The National Solar Radiation Data Base (NSRDB)," *Renewable and Sustainable Energy Reviews,* vol. 89, pp. 51-60, 2018/06/01/ 2018.

[15] J. S. Stein, W. F. Holmgren, J. Forbess, and C. W. Hansen, "PVLIB: Open source photovoltaic performance modeling functions for Matlab and Python," in *2016 IEEE 43rd Photovoltaic Specialists Conference (PVSC)*, 5-10 June 2016 2016, pp. 3425-3430, doi: 10.1109/PVSC.2016.7750303.

[16] J. S. Stein, "The photovoltaic Performance Modeling Collaborative (PVPMC)," in *2012 38th IEEE Photovoltaic Specialists Conference*, 3-8 June 2012 2012, pp. 003048-003052, doi: 10.1109/PVSC.2012.6318225.

[17] A. Dobos, "PVWatts Version 1 Technical Reference," National Renewable Energy Laboratory, Golden, CO., NREL/TP-6A20-60272, 2013.

[18] M. G. Deceglie, L. Micheli, and M. Muller, "Quantifying Soiling Loss Directly From PV Yield," *IEEE Journal of Photovoltaics,* vol. 8, no. 2, pp. 547-551, 2018, doi: 10.1109/JPHOTOV.2017.2784682.

[19] O. W. Westbrook, "Modeling maximum power point tracking efficiency for PV systems," in *2015 IEEE 42nd Photovoltaic Specialist Conference (PVSC)*, 14-19 June 2015 2015, pp. 1-4, doi: 10.1109/PVSC.2015.7356175.